Cell Stem Cell, Volume *28*

Supplemental Information

ROS Dynamics Delineate Functional States of Hippocampal Neural Stem Cells and Link to Their Activity-Dependent Exit from Quiescence

Vijay S. Adusumilli, Tara L. Walker, Rupert W. Overall, Gesa M. Klatt, Salma A. Zeidan, Sara Zocher, Dilyana G. Kirova, Konstantinos Ntitsias, Tim J. Fischer, Alex M. Sykes, Susanne Reinhardt, Andreas Dahl, Jörg Mansfeld, Annette E. Rünker, and Gerd Kempermann

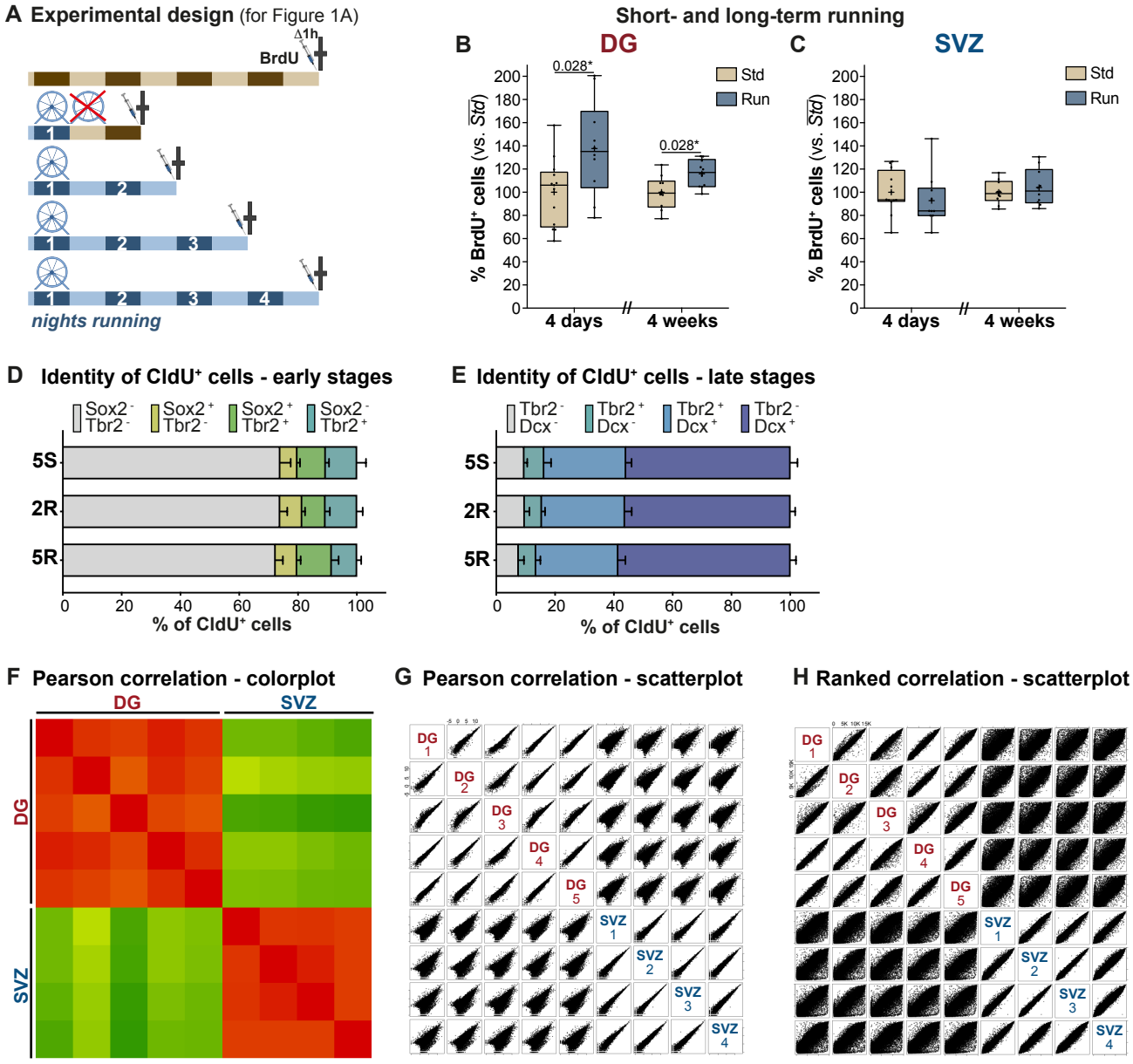

Figure S1 (related to figures 1 and 2): DG and SVZ differ in their response to physical activity. **(A)** Experiment outline for the paradigm analyzing the number of BrdU-labeled, proliferating cells after varying bouts of physical activity (result in Fig. 1A). **(B, C)** Relative comparison of BrdU$^+$ cells after a 4-day (short-term) and a 4-week (long-term) stimulus of running in the DG (B) and the SVZ (C). Note that while both durations of running significantly increase the pool of proliferating cells in the DG, a similar effect was not observed in the SVZ. Multiple t-tests with Holm-Sidak correction. **(D, E)** Extended data to Fig. 1B-F. The proportion of CldU$^+$ cells that are "early" (type-1 [Sox2$^+$] or type-2 [Sox2$^+$Tbr2$^+$] cells, D) and "late" in the neurogenic progression (type-2a [Tbr2$^+$], type-2b [Tbr2$^+$Dcx$^+$], or type-3 cells or post-mitotic immature neurons [Dcx$^+$], E). **(F-H)** Correlation analysis of the expression profiles of Nes-GFP$^+$ cells from the DG and the SVZ (see Fig. 2): (F) Pearson correlation color plot between samples collected from separate experiments; (G) scatterplot of the Pearson correlation between the samples; (H) scatterplot of the ranked correlation between samples. The horizontal line in the box plots indicates median and the "+" denotes mean. Bar plots show mean ± SEM. * $p < 0.05$. For further details in relation to replicate numbers, see Table S5.

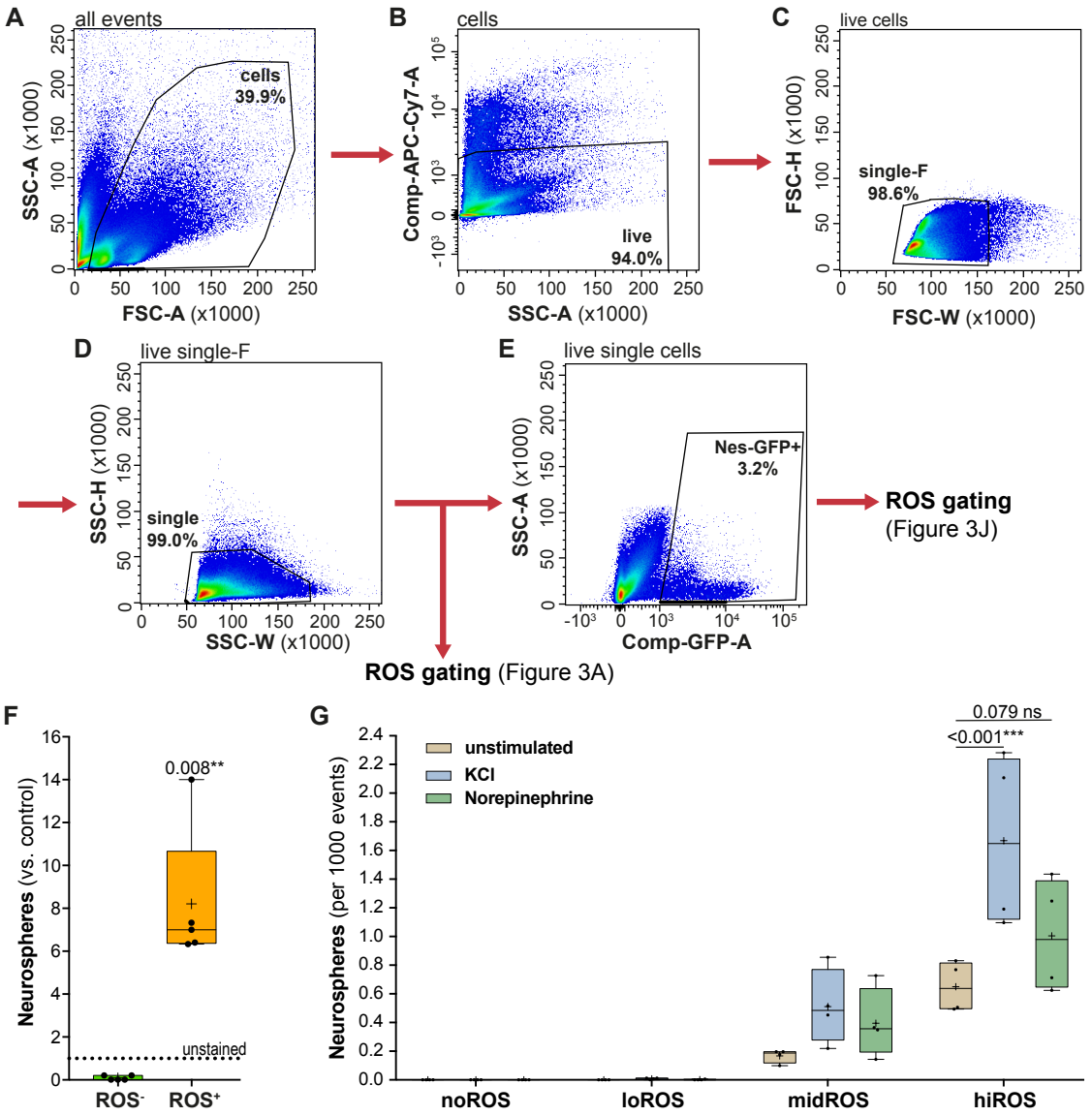

Figure S2 (related to figure 3): Gating Strategies for cytometric analyses and neurosphere assays. (A) All events were gated for forward (FSC-A; approximate of size) and sideward scatter (SSC-A; approximate of granularity) to exclude debris. **(B)** Cellular events were gated for putative live cells by exclusion of the viability dye eFluor 780 (APC-Cy7 filter; similarly, also PI was used as a viabilty dye). Cell doublets were excluded using the forward **(C)** and side **(D)** scatter signal properties (-Height vs -Width). Gating for ROS classes was applied to the live single cells (see Figure 3A) or, after a further gating step **(E)**, to the Nes-GFP$^+$ cells (see Figure 3J). **(F)** Isolated cells of the DG were gated and sorted according to two ROS classes (ROS$^-$ and ROS$^+$, not shown) to perform neurosphere assays. Neurosphere formation is restricted to the higher ROS class and significantly enriched compared to unstained sorted cells, one-sample t-tests. **(G)** Neurosphere formation from cells of each of four ROS classes (as in Fig. 3A) was assayed unstimulated or stimulated with KCl or Norepinephrine (NE). Irrespective of the stimulus, neurosphere formation was restricted to the mid and hiROS classes. Stimulation with either KCl or NE does not significantly change neurosphere formation in the midROS class. However, neurosphere formation from hiROS cells is strongly augmented by KCl stimulation ($p < 0.001$) and to a lesser extent by NE stimulation ($p = 0.079$). Two-way ANOVA with Dunnett post-hoc test. The horizontal line in the box plots indicates median and the "+" denotes mean. * $p < 0.05$, ** $p < 0.01$,*** $p < 0.001$. For details in relation to replicate numbers, see Table S5.

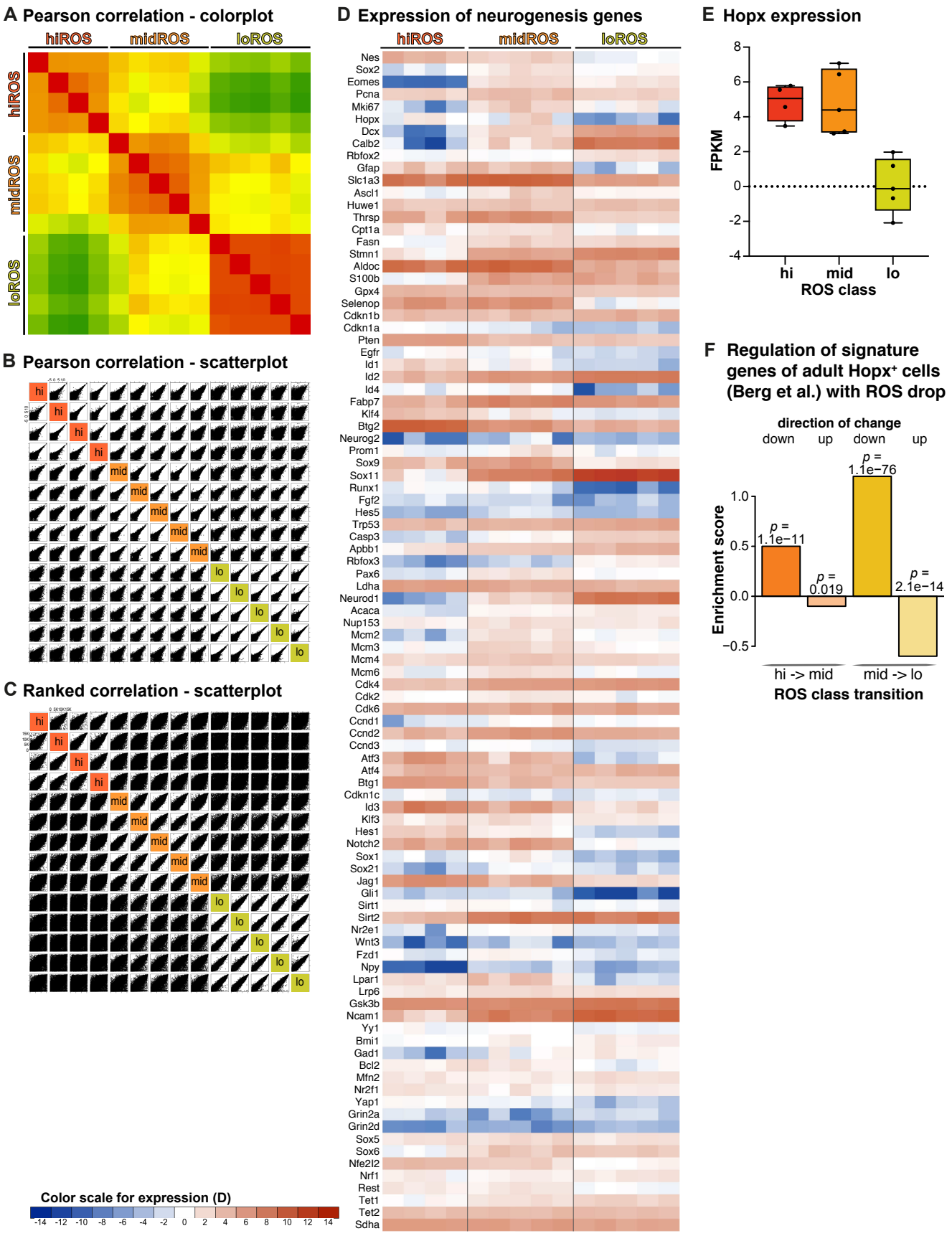

Figure S3 (related to figure 4)

Figure S3 (related to figure 4): Comparative analysis of the expression profiles of Nes-GFP$^+$ cells of the different ROS classes within the DG. (A) Pearson correlation color plot between the samples collected from separate experiments. **(B)** Scatterplots of the Pearson correlation between the samples. **(C)** Scatterplots of the ranked (Spearman) correlation between samples. **(D)** Heatmap showing the expression levels and the fold changes of curated transcripts with a known role in neurogenic maintenance and progression, and cell cycle regulation in the three ROS classes. Color scheme indicates level of expression (red high, blue low). **(E)** Expression levels of *Hopx* transcript within the three ROS classes. **(F)** Enrichment of genes identified by Berg et al. (2019) to be specifically upregulated in adult Hopx$^+$ cells at the two ROS drops. The hiROS class is indicated in red, midROS in orange and loROS in green.

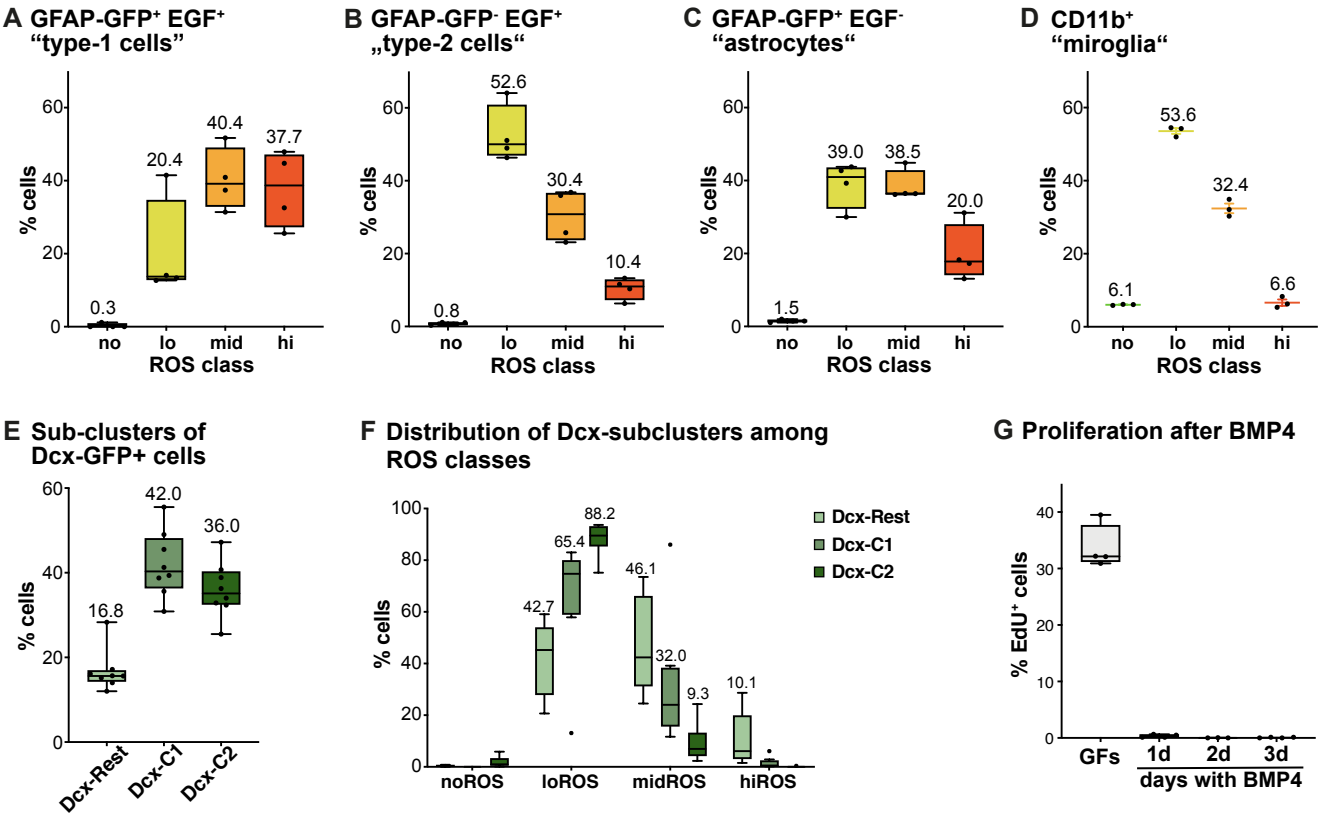

Figure S4 (related to figure 5): Cytometric segregation of different DG cell types into the four ROS classes. (A) Putative type-1 cells (Gfap-GFP$^+$ EGF$^+$). **(B)** Putative type-2 cells (Gfap-GFP$^-$ EGF$^+$). **(C)** Putative astrocytes (Gfap-GFP$^+$ EGF$^-$). **(D)** CD11b$^+$ microglia. **(E)** Relative abundance of identified subsets within Dcx-GFP$^+$ cells (see Fig. 5B). **(F)** Relative distribution of each of the Dcx-GFP$^+$ subsets into the different ROS classes. **(G)** Fraction of proliferating EdU$^+$ cells under control (GFs) and following BMP4 treatment in monolayer NPC cultures. All data represent mean percentages. The horizontal line in the box plots indicates median.

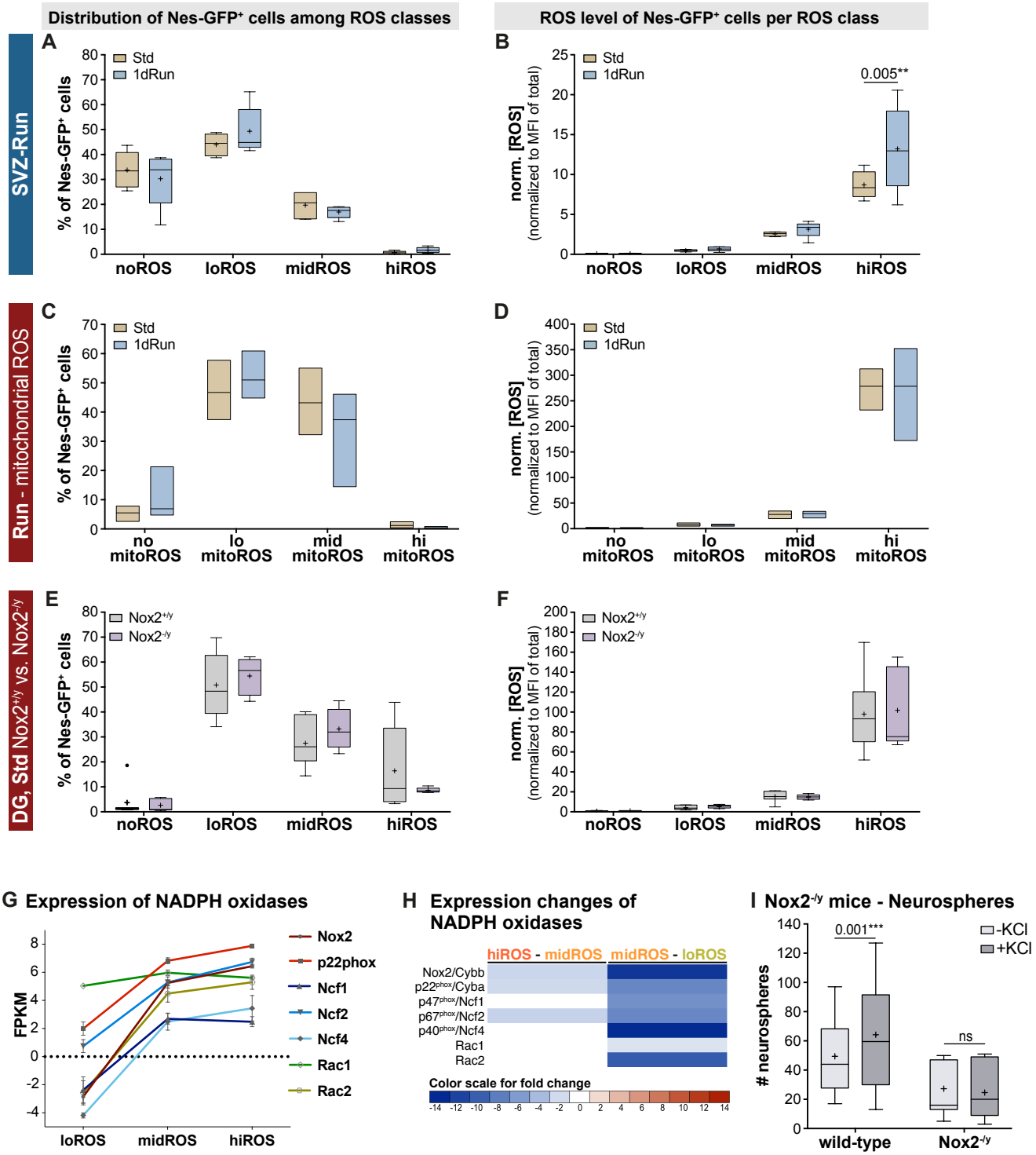

Figure S5 (related to figure 6)

Figure S5 (related to figure 6): Effects of physical activity in the DG are dependent on cellular Nox2. Distribution of Nes-GFP$^+$ cells of the SVZ among the different ROS classes **(A)** and their median intracellular ROS content **(B)** after 1 day of wheel running. Note that although a ROS surge, similar to the surge observed in hiROS Nes-GFP$^+$ cells of the DG (Fig. 6B), could be observed in the SVZ, this SVZ population is significantly smaller (~1%, Fig. 3L). Two-way ANOVA with Sidak post-hoc test. **(C-D)** The ROS changes of Nes-GFP$^+$ DG cells in response to exercise (see Fig. 6B) are not driven by mitochondrial activity, with no change observed in either the distribution of Nes-GFP$^+$ cells among the four mitoROS classes (C) nor the mitochondrial ROS content (D, n = 3). **(E, F)** Standard housed Nes-GFP::Nox2$^{-/y}$ mice and littermate Nes-GFP::Nox2$^{+/y}$ controls were analyzed with regard to the distribution of Nes-GFP$^+$ DG cells among ROS classes (E) and their median cellular ROS content (F), showing no differences. **(G)** Expression levels of Nox2 complex transcripts in Nes-GFP$^+$ cells of the different ROS classes. **(H)** Heatmap showing the significance of expression changes for different Nox2 transcripts at the two "ROS drops". **(I)** The number of neurospheres generated from the DG of wild-type and Nox2$^{-/y}$ mice was not significantly different; the addition of KCl only increased the neurosphere number from wildtype mice. Two-way ANOVA with Sidak post-hoc test. The horizontal line in the box plots indicates median and the "+" denotes mean. ** $p < 0.01$.

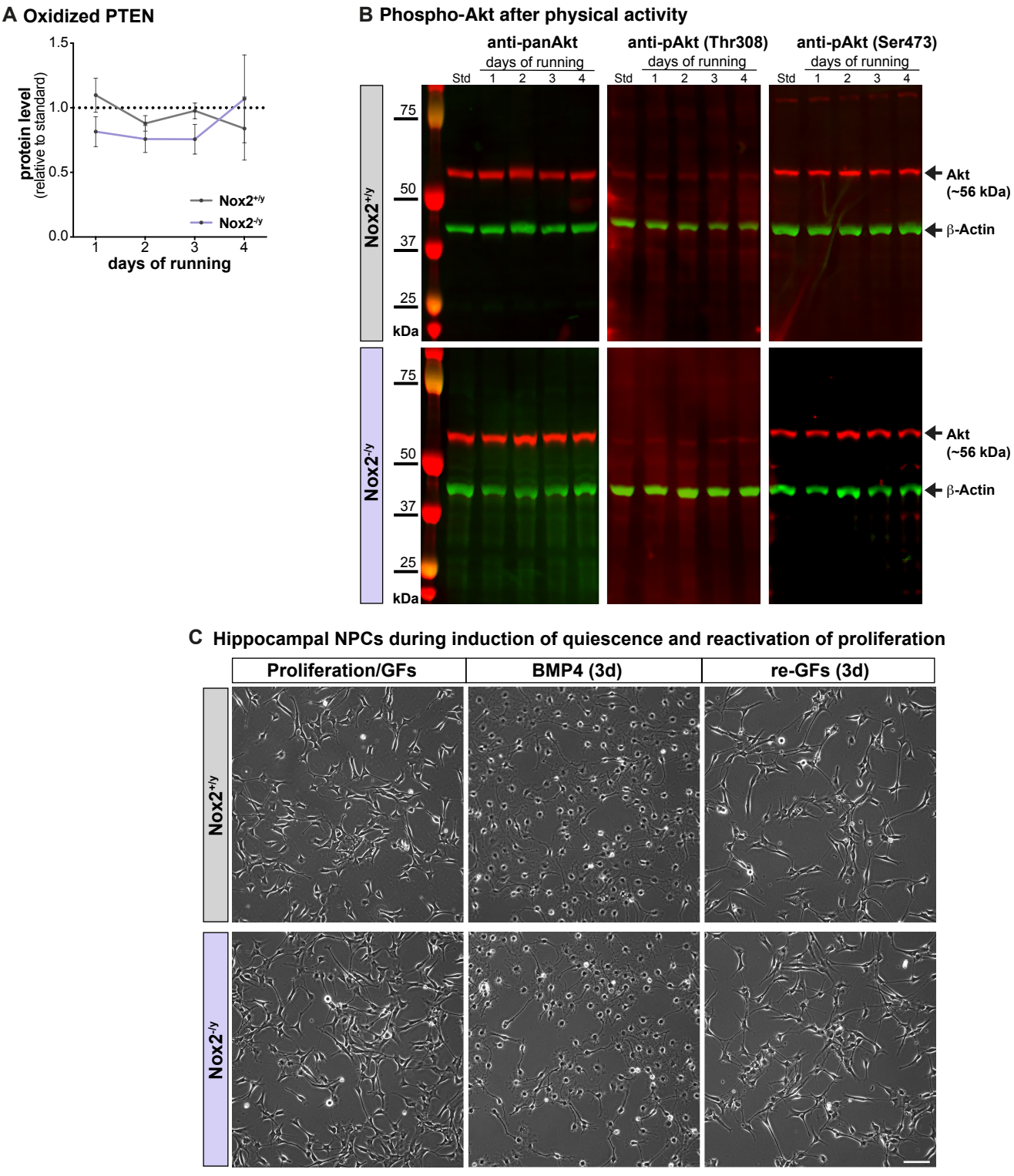

Figure S6 (related to figure 6): Western blotting and cell culture. (A) Levels of oxidized PTEN in total DG lysates after 1-4 days of physical activity, relativ to standard housed animals. **(B)** Western blotting for pan- and phospho-Akt (red) after 1-4 days of physical activity in Nox2$^{+/y}$ controls and Nox2$^{-/y}$ mutant mice. β-Actin (green) was used as an in-lane control and the Akt protein is visualized in red. **(C)** Brightfield images of Nox2$^{+/y}$ control and Nox2$^{-/y}$ mutant NPCs cultured under control proliferation conditions (GFs, left), 3 days of BMP4 (middle) and 3 days of reversion following BMP4 treatment (re-GFs, right). Scale bar: 50 µm.